Spin−Orbit Coupling Patterns Induced by Twist and Pyramidalization Modes in C_2H_4: A Quantitative Study and a Qualitative Analysis

David Danovich,[†] Christel M. Marian,[‡] Thomas Neuheuser,[‡] Sigrid D. Peyerimhoff,*,[‡] and Sason Shaik*,[†],[§]

Department of Organic Chemistry and the Lise Meitner-Minerva Center for Computational Quantum Chemistry, The Hebrew University, 91904 Jerusalem, Israel, and Institut für Physikalische und Theoretische Chemie, Universität Bonn, Wegelerstrasse 12, D-53115 Bonn, Germany

A study of the spin−orbit coupling (SOC) mechanisms which couple the triplet $\pi\pi^*$ state (T_1) to the singlet ground state (S_0) in ethylene is carried out at a variety of computational levels and basis sets, using the full Breit−Pauli (BP) SOC Hamiltonian, the one-electron mean-field (MF) operator, and the approximate one-electron operator based on an effective nuclear charge, Z^*. The basis set and wave functions requirements needed for good quality SOC calculations are elucidated by studying the SOC interaction using single- and multireference CI as well as MCSCF wavefunctions, with basis sets ranging from the minimal STO-3G all the way to an extended one with quadruple ζ and polarization quality. Two archetype distortion modes of ethylene were considered: a twist mode which changes the symmetry from D_{2h} to D_2 and then to D_{2d} and pyramidalization modes which change the ethylene symmetry to C_{2v} (syn-pyramidalization) or C_{2h} (anti-pyramidalization), as well as C_s (i.e., a mono-pyramidalization distortion). It is found that both the twist and syn-pyramidalization distortions of ethylene promote a nonzero SOC interaction, which involves an interplay between one-center and two-center SOC terms. In the twist distortion, the interplay is strong because the one-center terms arise from a residual incomplete cancelation of the two on-site interactions. In contrast, in the syn-pyramidalization distortion the interplay is weak, because the one-center terms add up. Consequently, the syn-pyramidalization promotes SOC matrix elements which exceed 6 cm^{-1}, while the twist mode has a weaker SOC on the order of 2 cm^{-1}. Zero SOC is obtained for distortion which involve either a 90° twist, or an anti-pyramidalization. The monopyramidalization distortion leads to SOC which is ca. 50% of that which is generated by the syn-pyramidalization. A qualitative analysis based on symmetry and electronic structure enables to understand these trends. A simple physical model, which enables us to carry out the vectorial summation of SOC in a pictorial manner, is constructed and used to explain the trends in the twist and syn-pyramidalization modes.

I. Introduction

There is a surge of interest in spin−orbit coupling (SOC)[1] interactions and their role in reactions which involve intersections of two states differing in their spin multiplicity.[2−17] Thus, it was postulated[3] that in triplet photoreactions, SOC determines the singlet product distribution which is nascent from the geometries which maximize the SOC between the triplet state T_1 and the singlet state S_0. Recent SOC calculations for a few triplet photochemical processes seem to be in line with this proposition.[6] More so, the role of SOC in gas phase reactions of transition metal ions with molecules has been amply demonstrated by experimental[12−14,16,17] and theoretical means.[15] A recent computational study of C−H/H−H bond activation by metal oxenide cations,[15] along with mass-spectrometric investigations,[16,17] have revealed that SOC influences both the reaction mechanism as well as the product distribution.[15a] Thus, not only is SOC a factor that affects the rate of a two-state reaction but it is also *a factor with structural and stereochemical consequences*. As such, there is a real need to develop

mechanistic insight into SOC interactions and to establish reliable and economical levels to compute these interactions. This is necessarily a long-term project which requires a stepwise buildup of insight and know-how. As a preliminary step for establishing the mechanistic significance of SOC in triplet organic reactions, we have selected as a benchmark case a simple and yet a fundamental problem the SOC patterns between the triplet $\pi\pi^*$ and the ground states (T_1 and S_0) of ethylene.

Triplet (T_1) ethylene and other unconstrained triplet olefins decay to the singlet ground state (S_0) by twisting around the C=C double bond.[1,4,7] Twisting is less likely to be the decay mechanism utilized by constrained olefins (e.g., **1** and **2**) which nevertheless possess
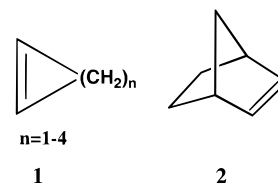

remarkably short triplet lifetimes.[7c,18] Therefore, to understand SOC patterns in olefins, it is necessary to explore the SOC interactions promoted by various archetypal distortions of the

---
[†] Department of Organic Chemistry and the Lise Meitner-Minerva Center for Computational Quantum Chemistry.
[‡] Institute für Physikalische und Theoretische Chemie.
[§] E-mail: sason@yfaat.ch.huji.ac.il or sason@shiva02.ch.huji.ac.il. FAX: +972-2-6585345.

double bond depicted in **3a**−**c**. Thus, in addition to the twist mode which has been analyzed

3a   **3b**

3c
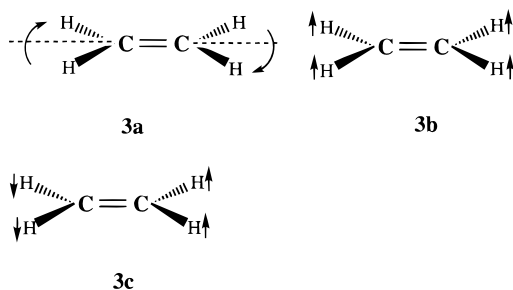
extensively[2,4,7,19] ever since the pioneering study of Salem and Rowland,[2] we shall study the pyramidalization modes **3b,c**. It was first pointed out by Shaik and Epiotis[3a] that pyramidalization of the olefinic centers promotes efficient and stereoselective T_1−S_0 SOC in triplet 2+2 cycloadditions and that it can thereby generate stereospecific cyclobutane products with retention of the stereochemical information. A related observation has been made recently by Caldwell et al.[7c] based on MCSCF ($\pi/\pi*$)-SOC calculations, which revealed that only the syn-pyramidalization, **3b**, mode promotes SOC, and that this SOC matrix element is larger than the maximal SOC promoted by the twist mode, **3a**. These interesting SOC patterns will be investigated extensively, in the present paper, by a variety of computational means in order to establish the SOC trends and understand their origins. Michl[4] pointed out recently that the two-center SOC interaction in ethylene and other diradicals is negligible in comparison with the one-center SOC interaction, and that the major conclusions of the pioneering Salem−Rowland model,[2] reached by invoking two-center terms, can in fact be derived by consideration of the one-center SOC terms alone. Following Michl's study[4] we have computed one- and two-center SOC for the different distortion modes, with a hope to establish the interplay of the SOC interactions for a given distortion. The extensive computational study will be followed by a qualitative model which shows the origins of the SOC patterns and provides some insight into the various trends.

The computational study uses different model spin−orbit Hamiltonians ($\mathbf{H}_{SO}$):[1] the full Breit−Pauli spin−orbit Hamiltonian ($\mathbf{H}_{SO}(BP)$),[1g,20] the approximate one-electron spin−orbit coupling Hamiltonian, where the nuclear charge is replaced by an effective charge, $Z*$($\mathbf{H}_{SO}(Z*)$),[21] and the recently developed mean-field spin−orbit Hamiltonian, ($\mathbf{H}_{SO}(MF)$),[22] where the one-electron spin−orbit operator is defined by averaging the two-electron contribution over the valence electrons. Since SOC, associated with nonspectroscopic states such as distorted ethylene, is not an observable, it is important to benchmark the calculations against some experimentally known situations, such as the states involved in the C, C^+, CH^+, and CH species. These calculations will generally test the various methods, to ensure the reliability of trends, and will specifically indicate whether or not a universal $Z*$ value for carbon can be used for the approximate one-electron method. Following these extensive calculations, a practically simple method for calculating SOC in related and larger systems will be proposed.

II. Methods

A. Technical Details. Geometry optimizations of S_0 and T_1 were carried out at the UCCSD(T)/cc-pVDZ level using the GAUSSIAN-94 package of programs.[23] State energies were determined at the UCCSD(T)/cc-pVDZ//UCCSD(T)/cc-pVDZ using GAUSSIAN-94 and at the multireference CI (MRCI)//

UCCSD(T)/cc-pVDZ (the double slash indicates the type of single-point calculation performed at the geometry following the double slash) using the Bonn package of programs.[24]

Spin−orbit coupling calculations have been performed routinely using STO-3G[23] and cc-pVDZ basis sets.[25] However, in a few cases (specified later), we have used a variety of basis sets, STO-3G, STO-6G, 6-31G, 6-31G*,[23] cc-pVDZ, TZP (the latter[26] consists of a 10s6p/[5s3p] contraction of Dunning plus a d-set on carbon with exponent 0.75, and a p-set on hydrogen with exponent 1.0), as well as a few basis sets from the MOLCAS library,[27] up to quadruple ζ with two sets of polarization functions and one set of f-functions.

B. SOC Methods. At the most rigorous level, the SOC matrix element is determined between two multireference CI (MRCI) wave functions with respect to the full Breit−Pauli spin−orbit operator[19,20] shown in eq 1, where the summation is over nuclei (κ) and electrons (i and j). The $\mathbf{r}_i \otimes \mathbf{p}_i$ product is the orbital angular momentum operator ($\mathbf{L}_i$), while $\mathbf{S}_i$ is the corresponding spin operator. Thus, the first term in eq 1 accounts for the one-electron interaction that each electron samples by "revolving" about all nuclei. The second term corresponds to the interaction of the angular momentum of an electron with the spins of other electrons. All the calculations employed the Bonn package of SO programs.[28]

$$\mathbf{H}_{SO}(BP) = \frac{\alpha^2}{2}\left\{\sum_i\sum_K\left(\frac{Z_K}{r_{iK}^3}\right)\mathbf{S}_i\cdot(\mathbf{r}_{iK}\otimes\mathbf{p}_i) - \sum_{i\neq j}\frac{1}{r_{ij}^3}(\mathbf{r}_{ij}\otimes\mathbf{p}_i)\cdot(\mathbf{S}_i+2\mathbf{S}_j)\right\} = \sum_i h_i(Z_k) + \sum_{ij}h_{ij}; \quad \frac{\alpha^2}{2} = \frac{e^2h}{4\pi m_e^2 c^2} \quad (1)$$

Approximate one-electron SOC calculations have been carried out with the GAMESS[29] suit of programs, using the effective one-electron SO operator,[21] in eq 2,

$$\mathbf{H}_{SO}(Z*) = \frac{\alpha^2}{2}\sum_i\sum_K\left(\frac{Z_K^*}{\mathbf{r}_{iK}^3}\right)\mathbf{S}_i\mathbf{L}_{iK} = \sum_i h_i(Z*) \quad (2)$$

where $\mathbf{L}_{iK}$ and $\mathbf{S}_i$ are the orbital and spin angular momentum operators for an electron i in the framework of the nuclei, indexed by K. To account for the missing two-electron part of the Hamiltonian, the nuclear charge Z_K is replaced by an effective parameter, Z_K^*, which can be taken as the screened nuclear charge,[1a,21] and it is treated as a parameter to be determined by calibration of the SOC calculations with respect to an observable value.

The mean-field SO operator, $\mathbf{H}_{SO}(MF)$, has been described recently.[22] It is an effective one-electron operator achieved by averaging over the two-electron interactions, similar to the Coulomb and exchange operators in Hartree−Fock theory. By construction, matrix elements of this operator occur only between valence orbitals; a representative one is shown in eq 3.

$$H_{ij}^{\text{mean field}} = \langle i|\mathbf{H}_{SO}(1)|j\rangle + \frac{1}{2}\sum_{\substack{k \\ \text{fixed}\{n_k\}}} n_k\{\langle ik|\mathbf{H}_{SO}(1,2)|jk\rangle - \langle ik|\mathbf{H}_{SO}(1,2)|kj\rangle - \langle ki|\mathbf{H}_{SO}(1,2)|jk\rangle\} \quad (3)$$

Herein, i and j denote valence spin orbitals, the $\sum_k$ runs over all core and selected valence spin orbitals, and n_k stands for the

Spin−Orbit Coupling Patterns

J. Phys. Chem. A, Vol. 102, No. 29, 1998 **5925**

occupation of orbital k. Typically, the valence orbitals occupied in a Hartree−Fock configuration are included in the mean-field summation. Thus, instead of treating the screened nuclear charge as a parameter, the $H_{SO}(MF)$ views it as quantity that ultimately depends on the specific molecular environment, and as such $H_{SO}(MF)$ is a better approximation than the $H_{SO}(Z^*)$, to the full Breit−Pauli Hamiltonian in eq 1.

For a Hartree−Fock wave function this mean-field approximation reproduces exactly the result of the corresponding full spin−orbit Hamiltonian. Thus, it has been shown[22] that it approximates the results of the full operator very well if single excitations dominate in the expansion of the CI wave functions. This mean-field spin−orbit approximation has primarily been developed to be used for calculating spin-dependent properties of heavy element compounds. For second- and third-row transition metal atoms, the choice of valence orbital occupations n_k is not critical.[22] This might be different for light elements like carbon where the two-electron part contributes approximately 50% to the total spin−orbit matrix element. For the present case of C_2H_4 we tested various valence orbital occupations at a geometry with the C−C bond twisted by 50°. In each specification of the mean field, the lower lying α and β spin orbitals (corresponding to 1a, 2a, 3a, 1b$_l$, 1b$_2$, 1b$_3$, and 2b$_3$) were each singly occupied, while for the π and π^* orbitals variable occupations were tested, in the following three options:

(a) π^2: 1.0 2b$_2$ α, 1.0 2b$_2$ β

(b) π^{*2}: 1.0 2b$_1$ α, 1.0 2b$_1$ β

(c) $\pi\pi^*$: 0.5 2b$_2$ α, 0.5 2b$_2$ β, 0.5 2b$_1$ α, 0.5 2b$_1$ β

With this choice of mean-field orbitals, we obtained the following values for the spin−orbit matrix element between the singlet ground state and the first excited triplet state of ethene which may be compared to a value of 2.18 cm^{-1} for the full Breit−Pauli Hamiltonian in the same basis at 50° twisting: 2.22 cm^{-1} (case a), 2.24 cm^{-1} (case b), and 2.23 cm^{-1} (case c).

Calibration of the SOC Calculations and Finding Z^* Values. To establish a reliable level for the SOC(BP) calculations, as well as for determining the value of Z^* required to use in the approximate one-electron method, SOC matrix elements have been calculated for a few fragments: C, C$^+$, CH, and CH$^+$, for most of which experimental data is available.[30]

Full valence MRCI calculations were carried out for CH-(X$^2\Pi$) and CH$^+$(a$^3\Pi$) with cc-pVDZ and TZP basis sets. Spin−orbit matrix elements were evaluated employing both the full Breit−Pauli Hamiltonian and its mean-field approximated form. CASSCF orbitals were optimized for the a$^4\Sigma^-$ state of CH by distributing the 5 valence electrons in 5 active orbitals: using this one-particle basis the reference space for CH(X$^2\Pi$) comprised 11 configurations. In the CI expansion of the CH-(X$^2\Pi$) wave function the leading configuration $(1\sigma^2 2\sigma^2 3\sigma^1 1\pi^1)$ has a weight (c^2) of 0.92 while the squared coefficients of the other 10 reference configurations sum up to 0.05. The calculated Breit−Pauli spin−orbit matrix elements for CH(X$^2\Pi$) were 12.0 cm^{-1} with cc-pVDZ and 13.1 cm^{-1} with TZP, as well as with seven other basis sets of increasing size the value converges to 13.4 cm^{-1}, whereas experiment gives 14.0 cm^{-1}.[30] Using the mean-field spin−orbit Hamiltonian, constructed with orbital occupations derived from the leading configuration, gave 12.3 cm^{-1} (cc-pVDZ) and 13.2 cm^{-1} (TZP), in good accord with the Breit−Pauli results.

The situation is somewhat different in the case of CH$^+$(a$^3\Pi$). Here, full-valence active space orbitals were optimized for the X$^1\Sigma^+$ state of CH$^+$ (4 electrons in 5 active orbitals) and 10 reference configurations were used as generators for the MRCI space of CH$^+$(a$^3\Pi$). The leading configuration $(1\sigma^2 2\sigma^2 3\sigma^1 1\pi^1)$ is less dominant ($c^2 = 0.77$) in this case and a second prominent configuration $(1\sigma^2 2\sigma^1 3\sigma^2 1\pi^1)$ contributes a weight of 0.15. Again, the total weight of the reference vector in the CI expansion amounts to 0.97. The full Breit−Pauli SOC matrix element for CH$^+$($^3\Pi$) was calculated to be 15.4 cm^{-1} with cc-pVDZ and 16.6 cm^{-1} with TZP. Larger basis sets[27] show that the value converges to 16.6 cm^{-1}. The 23.0 cm^{-1} value, which appears in experimental tables is in fact an old theoretical estimate, and we propose that the presently calculated value of 17−18 cm^{-1} is more accurate. Using the mean-field approximation, the matrix elements are within this range (i.e., 16.7 cm^{-1} with cc-pVDZ and 18.0 cm^{-1} with TZP).

Using these benchmark values we proceeded to find a Z^* value to be used with the approximate one-electron method. Earlier determination by Koseki et al.[21a] showed that with the 6-31G basis set a value of $Z^* = 3.6$ reproduces the multiplet splitting in both CH and CH$^+$. To test the applicability of this Z^* value, we used two different basis sets, cc-pVDZ and STO-3G, coupled with full valence MCSCF calculations. For the $^2\Pi$ state of CH, a SOC matrix element of 15.8 cm^{-1} is obtained with cc-pVDZ, as well as with STO-3G, in comparison with 14.0 cm^{-1} evaluated from experiment and 13.4 cm^{-1} calculated with the BP Hamiltonian. For the CH$^+$($^3\Pi$) species, the one-electron method gave a matrix element of 20.6 cm^{-1} with cc-pVDZ and 16.5 cm^{-1} with STO-3G, in comparison with 17−18 cm^{-1}, the corrected value suggested above. Using the same Z^* and basis sets for C$^+$(^{2}P), the calculated SOC matrix elements are 22.4 cm^{-1} with cc-pVDZ and 16.6 cm^{-1} with STO-3G in comparison with an experimental value[31] of 21.3 cm^{-1}. For C(^{3}P), the resulting matrix elements are 16.9 cm^{-1} with cc-pVDZ and 16.6 cm^{-1} with STO-3G in comparison with a 16.4 cm^{-1} experimental value.[31] It appears that, while the $Z^* = 3.6$ value is not a constant, it is nevertheless a reasonable value which shows remarkably small dependence on basis set. Thus, as long as we are dealing with one-center situations such as the fragments discussed above, the approximate one-electron method gives reasonable results even with the STO-3G basis set.

C. T$_1$−S$_0$ SOC Calculations for C$_2$H$_4$. *MRCI/SO(BP) Calculations.* In the MRCI calculations for the singlet ground state and the first excited triplet state of ethene, a common set of triplet π to π^* ROHF orbitals has been employed as one-particle basis. These molecular orbitals have the advantage that they conserve the symmetry of the molecular wave function for twist and syn-pyramidalization modes.

SOC for Twist Mode (**3a**). This mode has been studied for twist angles between 0° and 90°, at 10° intervals. The electronic calculations involve three reference configurations, π^2, $\pi^2 \rightarrow \pi^{*2}$, and $\sigma_{CH} \rightarrow \pi^*$, for the singlet state while only one ($\pi \rightarrow \pi^*$) for the triplet state. All valence electrons in 46 orbitals (12 of symmetry a and b$_3$, respectively, and 11 of symmetry b$_1$ and b$_2$, respectively) are correlated. With a threshold of zero in the selection procedure, there result 27 505 CSFs for S$_0$ and 26 607 for T$_1$, using the cc-pVDZ basis set. At a threshold of 5 μhartrees, the number of CSFs drops to ca. 8000, but the SOC is affected by less than 0.1 cm^{-1}. The resulting S$_0$ wave function shows a dominance of the π^2 and π^{*2} configurations, with a weight of 0.904−0.908, while the T$_1$ wave function is dominated by the $\pi\pi^*$ configuration with weights

of 0.9094−0.9127, for various twist angles. These wave functions are then used for the calculations of the $\langle T_1|\mathbf{H}_{SO}\text{-}(BP)|S_0\rangle$ matrix element.

SOC for the Pyramidalization Mode (**3b**). This mode has been studied for angles between 10 and 90° at 10° intervals. The MRCI involved five reference singlet configurations which are π^2, $\pi^2 \rightarrow \pi^{*2}$, $\sigma_{CH} \rightarrow \pi^*$, $(\sigma_{CH},\pi) \rightarrow \pi^{*2}$, and $(\sigma_{CH},\pi) \rightarrow (\pi^*,\pi'^*)$, and a single triplet reference, $\pi \rightarrow \pi^*$. All valence electrons in 46 orbitals, 14 with a_1 and b_1 symmetry, respectively, and 9 with a_2 and b_2 symmetry, respectively were correlated using a threshold of 5 μhartrees for the selection and resulting in 6200−6700 CSFs for S_0 and 9500−9700 for T_1. The weight of the five reference configurations reaches 0.8998−0.9066, while the triplet reference has a weight of 0.9052−0.9122. Testing a singlet with three reference ("3-main") configurations as in the calculation for the twist mode, leads to a SOC matrix element which is 0.2 cm^{-1} smaller than the result of the "5-main" calculations. A "5-main" calculation with zero threshold seemed too expensive and was not attempted, but a test of accuracy was conducted using the "3-main" wave function with a zero threshold, which was found to change the SOC matrix element by only ca. <0.02 cm^{-1}. Furthermore, adding an additional reference configuration to S_0, due to $\sigma_{CC} \rightarrow \sigma_{CC}^*$ excitation, increases the combined weight by only 0.0044 (for a pyramidalization angle of 70°), and changes the SOC value from 5.30 cm^{-1} to 5.35 cm^{-1}. It is concluded therefore, that the "5-main" wave function with 5 μhartrees threshold is of sufficient accuracy for SOC calculations.

SO(Z*) Calculations. Approximate one-electron (eq 2) SOC calculations are performed as a SO-CI between T_1 and S_0: themselves predetermined by CI or MCSCF (m/n) calculations (m is the number of electrons and n the number of orbitals). The T_1 and S_0 states involve the same set of orbitals which are usually the orbitals of the singlet state. In one case we use the orbitals of the triplet state. In the latter case, the T_1 state is calculated by the ROHF method, and the triplet orbitals undergo Boys localization. The resulting MOs and hybrids serve subsequently as a basis for CI-SO(Z*) calculations.

MRCI-SO(MF) Calculations. The electronic calculations are precisely as described above for the MRCI-SO(BP) calculations, while the SOC matrix elements are calculated with the effective one-electron Hamiltonian which implicitly includes the two-electron effect via a mean field which is defined by specifying orbital occupation numbers.[22] Different mean-fields were tested, for example, with valence orbital occupations π^2, π^{*2}, and $\pi^1\pi^{*1}$. The results were only marginally dependent on the valence orbital occupation, and Tables 4 and 5 show the results with the $\pi^1\pi^{*1}$ mean field. The TZP basis set was used throughout.

Partition of the SOC Matrix Elements. To gain insight into the SOC patterns, all the $\mathbf{H}_{SO}$ matrix elements were analyzed in terms of one- and two-center interactions. In addition, the $\mathbf{H}_{SO}(BP)$ matrix elements were partitioned into their one- and two-electron components.

III. Results

A. Geometry and Energies of S_0 and T_1. Table 1 shows the optimized geometric parameters of the two states, along the syn-pyramidailization and the twist modes, following the definitions in Scheme 1. No optimization was carried out along the mono- or anti-pyramidalization modes. Table 1 shows that the singlet state undergoes progressive C−C elongation, during the twist mode, while the triplet state undergoes bond shortening. This difference reflects undoubtedly the bonding features in the

TABLE 1: Optimized Geometric Parameters (in angstroms) of Ethylene during Pyramidalization and Twist Motions

| | T_1 | | S_0 | |
| | syn-pyramidalization(sp) | twist(t) | twist(t) | |
Θ^a	$R(C=C)^b$	$R(C=C)^c$	$R(C=C)^d$	$R(C=C)^e$
0	1.5507	1.5506	1.3516	1.3060
10	1.5507	1.5480	1.3526	1.3067
20	1.5506	1.5287	1.3555	1.3090
30	1.5527	1.5283	1.3606	1.3128
40	1.5582	1.5137	1.3683	1.3184
50	1.5682	1.4995	1.3794	1.3260
60	1.5876	1.4865	1.3951	1.3361
70	1.6199	1.4765	1.4188	1.3492
80	1.6719	1.4720	1.4547	1.3665
90^f	1.7494	1.4682	1.4968	1.3899

^{a} The angle of the distortion in degrees. ^{b} The T_1 state was optimized using UCCSD(T)/cc-pVDZ level of theory. ^{c} The T_1 state was optimized using UCCSD(T)/cc-pVDZ level of theory. ^{d} The S_0 state was optimized using CCSD(T)/cc-pVDZ level of theory. ^{e} The S_0 state was optimized using HF/STO-3G level of theory. ^{f} The angle Θ was fixed at 89.9° for the twist distortion.

SCHEME 1
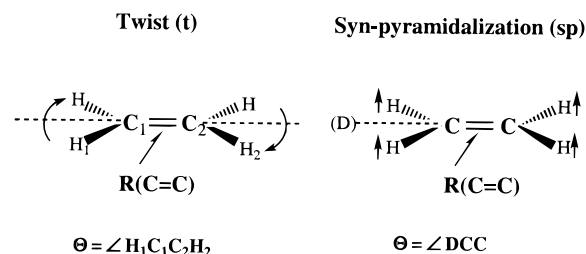
two states: the loss of bonding in S_0 causes bond elongation, while the release of triplet exchange repulsion in T_1 causes bond shortening. Along the pyramidalization mode, the triplet state exhibits progressive C−C elongation, which reflects the strong mixing of π and σ, and the onset of conversion of the T_1 state of C_2H_4 into a composite of one-triplet and one -singlet carbenes.

Tables 2 and 3 show the total energy and S_0−T_1 vertical energy gap (at T_1 geometries), as a function of the distortion coordinates. It is apparent that MRCI and CCSD(T) energy gaps are very close, both exhibiting a consistent picture of a gradual decrease of the gap. However, while the twist mode causes state crossing, in the pyramidalization mode the states remain separated by an energy gap of ca. 0.8 eV.

B. SOC Results for C_2H_4. *MCSCF and MRCI Results.* Tables 4 and 5 show the $\langle T_1|\mathbf{H}_{SO}|S_0\rangle$ results, henceforth $\langle SOC\rangle$, for the three model Hamiltonians defined by eqs 1−3, at the respective wave function levels. The $\langle SOC(Z^*)\rangle$ results were obtained at MCSCF(12/12) levels including 12 valence electrons in 12 orbitals, while the $\langle SOC(BP)\rangle$ and $\langle SOC(MF)\rangle$ results correspond to MRCI wave functions.

Table 4 shows the variation of $\langle SOC\rangle_t$, along the twist mode, in Scheme 1. All the methods indicate that $\langle SOC\rangle_t$ peaks around 50−60°, and then diminishes to zero. The final nonzero value of $\langle SOC(BP)\rangle_t$ is due to the fact that the calculation was done at 89.9°. The maximum $\langle SOC(BP)\rangle_t$ value shows some dependence on the basis set and increase from 1.58 at the cc-pVDZ basis set to 1.89 cm^{-1} at the TZP basis set. Since a larger basis set is too demanding, we may consider the $\langle SOC(BP)\rangle_t$/TZP results as benchmark values. In this sense, the $\langle SOC(Z^*)\rangle_t$ at the larger basis sets, and the $\langle SOC(MF)\rangle_t$ are in good match with the benchmark values. A one-electron operator is deemed reliable when coupled with a good quality wave function and a large enough basis set.

Spin−Orbit Coupling Patterns

J. Phys. Chem. A, Vol. 102, No. 29, 1998 **5927**

TABLE 2: Total Energy (−78.0 au) and Singlet−Triplet Energy Gap (ΔE) for Ethylene during the Twist Distortion at the CCSD(T)/cc-pVDZ and MRSDCI/cc-pVDZ Levels of Calculations

geometry,[a] Θ	$E_{CCSD(T)}$, au		$\Delta E_{CCSD(T)}$, eV	E_{MRD-CI},[b] au		ΔE_{MR-CI},[c] eV
	$X^1A_1(S_0)$	$a^3B_3(T_1)$	$X^1A_1 \rightarrow a^3B_3$	$X^1A_1(S_0)$	$a^3B_3(T_1)$	$X^1A_1 \rightarrow a^3B_3$
T_1, 0	0.329157	0.226337	2.80			
T_1, 10	0.328299	0.227103	2.75			
T_1, 30	0.320651	0.232795	2.39			
T_1, 40	0.313019	0.237119	2.07	0.28107	0.20792	1.99
T_1, 50	0.302119	0.241791	1.64	0.27037	0.21252	1.57
T_1, 60	0.288249	0.246229	1.14	0.25708	0.21688	1.09
T_1, 70	0.272323	0.249865	0.61			
T_1, 90	0.250545	0.253068	−0.07	0.22462	0.22360	0.03

[a] UCCSD(T)/cc-pVDZ optimized geometry at variable angle Θ (Scheme 1) for triplet T_1 state. [b] These values are obtained with the zero selection threshold. [c] The corresponding values, for the first three entries, with the TZP basis set are 1.98, 1.55, 1.07 eV.

TABLE 3: Total Energy (−78.0 au) and Energy Gap (ΔE) for Ethylene during the Syn-Pyramidalization Distortion at the CCSD(T)/cc-pVDZ and MRSDCI/cc-pVDZ Levels of Calculations

geometry,[a] Θ	$E_{CCSD(T)}$, au		$\Delta E_{CCSD(T)}$, eV	E_{MRD-CI},[b] au		ΔE_{MR-CI},[c] eV
	$X^1A_1(S_0)$	$a^3B_2(T_1)$	$X^1A_1 \rightarrow a^3B_2$	$X^1A_1(S_0)$	$a^3B_2(T_1)$	$X^1A_1 \rightarrow a^3B_2$
T_1, 0	0.329157	0.226337	2.80			
T_1, 10	0.327575	0.226711	2.75			
T_1, 30	0.313849	0.227622	2.35			
T_1, 40	0.300993	0.225697	2.05	0.26899	0.19650	1.97
T_1, 50	0.283939	0.220231	1.73	0.25181	0.19129	1.65
T_1, 60	0.262865	0.210034	1.44	0.23060	0.18044	1.36
T_1, 70	0.237932	0.194374	1.19	0.20503	0.16403	1.12
T_1, 90	0.179307	0.147419	0.87	0.21435	0.11436	0.79

[a] UCCSD(T)/cc-pVDZ optimized geometry at variable angle Θ for the T_1 state. [b] See corresponding comment in Table 2. [c] TZP results are virtually identical.

TABLE 4: Dependence of the Spin−Orbit Coupling on the Basis Sets and the Type of Calculations for the Twist Distortion at the T_1 Optimized Geometries

	spin−orbit coupling, $|\langle S_0|H_{SO}|T_1\rangle|$, cm^{-1}								
	$\langle SOC(Z^*)\rangle_t$, MCSCF(12/12)[a]						$\langle SOC(BP)\rangle_t$, MRD-CI[b]		$\langle SOC(MF)\rangle_t$, MRD-CI[c]
geometry, Θ	STO-3G	STO-6G	6-31G	6-31G*	TZP	cc-pVDZ	cc-pVDZ	TZP	TZP
T_1, 0	0.0	0.0	0.0	0.0		0.0	0.0	0.0	0.0
T_1, 10	0.16	0.17	0.44	0.46		0.48			
T_1, 30	0.44	0.46				1.33			
T_1, 40	0.54	0.57			1.99	1.64	1.43	1.71	1.75
T_1, 50	0.59	0.62	1.69	1.70	2.22	1.81	1.57	1.88	1.93
T_1, 60	0.58	0.61			2.27	1.83	1.58	1.89	1.93
T_1, 70	0.49	0.51	1.50	1.46		1.60			
T_1, 80	0.29	0.30	0.81	0.81		0.92			
T_1, 90	0.0	0.0	0.0	0.0		0.0	0.02		

[a] $Z^* = 3.6$. [b] H_{SO} is Breit−Pauli 1e+2e operator. [c] H_{SO} is the mean-field one-electron operator.

TABLE 5: Dependence of the Spin−Orbit Coupling on the Basis Sets and the Type of Calculations for the Syn-Pyramidalization Distortion at the T_1 Optimized Geometries[a,b]

	spin−orbit coupling, $|\langle S_0|H_{SO}|T_1\rangle|$, cm^{-1}							
	$\langle SOC(Z^*)\rangle_{sp}$, MCSCF(12/12)					$\langle SOC(BP)\rangle_{sp}$, MRD-CI		$\langle SOC(MF)\rangle_{sp}$, MRD-CI
geometry, Θ	STO-3G	STO-6G	6-31G	TZP	cc-pVDZ	cc-pVDZ	TZP	TZP
T_1, 0	0.0	0.0	0.0		0.0	0.0	0.0	0.0
T_1, 10	1.09	1.15	1.38		1.43			
T_1, 30	3.02	3.19	3.86		4.02			
T_1, 50	4.36	4.60	5.68	5.49	5.99	4.50	4.83	4.86
T_1, 70	5.23	5.52	6.96	7.21	7.47	5.30	5.82	5.85
T_1, 90	5.87	6.16	7.82	8.70	8.60	5.77	6.29	6.33

[a] Anti-pyramidalization possesses $\langle SOC\rangle_{ap} = 0$. [b] Using STO-3G, it is found that mono-pyramidalization promotes about 50% of the total $\langle SOC(Z^*)\rangle_{sp}$.

The basis set effect was explored using the approximate one-electron Hamiltonian, and the results are exhibited under the $\langle SOC(Z^*)\rangle_t$ column. The STO-NG basis sets give correct qualitative trends, but their quantitative results are quite poor. Starting with the 6-31G basis set, one obtains reasonable quantitative results, too. Similar conclusions were noted before by Klotz et al.[32] for SOC in the SO molecule. The poor performance of the STO-3G stands in contrast with its good performance in the monocarbonized species, CH, CH⁺, C, and C⁺, and implies that the problem of small basis sets must originate, not from the one-center $\langle SOC\rangle$ terms *but from the interference of two-center terms.* As shown later, this interference is reproduced also with the rigorous BP Hamiltonian.

5928 *J. Phys. Chem. A, Vol. 102, No. 29, 1998*

Danovich et al.

TABLE 6: Dependence of the Spin−Orbit Coupling (cm⁻¹) on the Type of CI Calculations upon Twist Distortion[a]

	$\langle SOC(Z^*)\rangle_t$/STO-3G		
geometry,[b] Θ	CISD(12/12)	CISDT(12/12)	CISDTQ(12/12)
S_0, 0	0.0	0.0	0.0
S_0, 10	0.31	0.39	
S_0, 30	0.80	0.95	
S_0, 40	0.93	1.08	1.02
S_0, 50	0.98	1.13	1.04
S_0, 60	0.96	1.09	
S_0, 70	0.87	0.96	
S_0, 90	0.35	0.34	0.00

[a] Only 1s electrons were excluded from CI calculations. [b] The geometries correspond to S_0 at the RHF/STO-3G level of theory.

TABLE 7: Dependence of the Spin−Orbit Coupling (cm⁻¹) on the Type of CI Calculations upon Twist Distortion

	$\langle SOC(Z^*)\rangle_t$/cc-pVDZ[a,b]		
geometry,[c] Θ	CISD(12/48)	CISDT(12/16)	CISDTQ(12/16)
T_1, 0	0.0	0.0	0.0
T_1, 10	0.55 (0.56)	0.52 (0.66)	0.51
T_1, 30	1.57 (1.70)	1.46 (1.73)	1.42
T_1, 50	2.35 (2.52)	2.09 (2.30)	2.00 (2.88)
T_1, 70	2.79 (2.92)	2.15 (2.36)	1.91
T_1, 90	2.81 (2.91)	0.91 (1.17)	0.34 (0.34)

[a] HF/STO-3G optimized geometry of S_0 state was used for the results which are presented in the parenthesizes. [b] Only 1s electrons were excluded from these calculations. [c] The geometries correspond to the T_1 state at the UCCSD(T)/cc-pVDZ level of theory.

TABLE 8: Dependence of the Spin−Orbit Coupling (cm⁻¹) on the Type of CI Calculations upon Syn-Pyramidalization Distortion

	$\langle SOC(Z^*)\rangle_{sp}$/cc-pVDZ[a]		
geometry,[b] Θ	CISD(12/48)	CISDT(12/16)	CISDTQ(12/16)
T_1, 0	0.0	0.0	0.0
T_1, 10	1.28	1.14	1.11
T_1, 30	3.77	3.21	3.14
T_1, 50	6.05	4.96	4.85
T_1, 70	8.21	6.62	6.38
T_1, 90	10.05	8.14	7.81

[a] Only 1s electrons were excluded from these calculations. [b] The T_1 state optimized geometry at the UCCSD(T)/cc-pVDZ level of theory.

Table 5 collects the results for the pyramidalization modes. First, the anti-pyramidalization mode (**3c**) has $\langle SOC\rangle_{ap} = 0$ independently of the pyramidalization angle. In contrast, the syn-pyramidalization promotes a significant $\langle SOC\rangle_{sp}$, in line with the results of Caldwell et al.[7c] We have also carried out a mono-pyramidalization (mp) distortion, where only one CH_2 group undergoes pyramidal distortion. The resulting $\langle SOC\rangle_{mp}$ is 50% of $\langle SOC\rangle_{sp}$ for a given angle. Thus, *the $\langle SOC\rangle_{mp}$ terms on the CH_2 termini add up in the syn mode and subtract in the anti mode.* Another important trend in Table 5 is the good performance of the STO-NG basis sets, in contrast with their very poor performance for the twist mode. This, as well as the additivity relationship of the mono-pyramidalization $\langle SOC\rangle_{mp}$ terms, provides a strong indication that the $\langle SOC\rangle_{sp}$ is dominated by one-center SOC.

C. $\langle SOC(Z^*)\rangle$ Results with Truncated and Minimal CI Wave Functions. SOC with CISD, CISDT, and CISDTQ Wave Functions. Since full valence MCSCF are not practical for large systems, we sought for a cheaper CI based method. The $\langle SOC(Z^*)\rangle$ results are summarized in Tables 6−8 for twist and pyramidalization distortions. Table 6 and 7 collect the results for the twist mode using STO-3G and cc-pVDZ basis
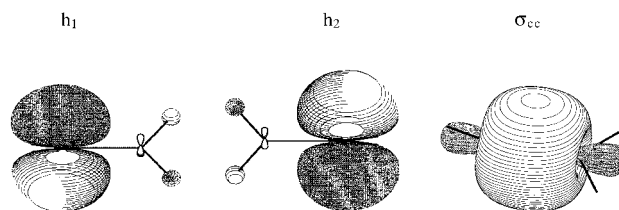
Figure 1. The h_1, h_2 hibrids and σ_{CC} orbital of C_2H_4 during the twist distortion.

sets. It is seen that SOC calculated on the basis of a *single reference CI wave function* is poor, since it predicts wrongly a significant $\langle SOC\rangle_t$, even at 90° of twist. As the basis set becomes larger, the results deteriorate even further, and CISD/cc-pVDZ predicts $\langle SOC(Z^*)\rangle_t = 2.8$ cm⁻¹ at 90°. Even after inclusion of triple and quadruple excitations, the 90° value is 0.34 cm⁻¹.

To verify that this poor behavior is associated with the CI wave function, we computed also $\langle SOC(BP)\rangle_t$ values using a CISD wave function, and found for 90° a large value, $\langle SOC(BP)\rangle_t = 2.06$ cm⁻¹. Thus, the difficulty is not with the nature of the SO Hamiltonian, but rather with the quality of the wave function. The problem of the CISD (or CISDTQ) expansion becomes apparent by noting that the wave function at 90° is dominated by the π^2 configuration which possesses a weight of 0.875 (with cc-pVDZ), in contrast with both MRCI and MCSCF wave functions which possess identical weights for π^2 and π^{*2} configurations. We recall[2,4] that at 90° the S_0 wave-function is a pure diradical which requires identical coefficients of the π^2 and π^{*2} configurations. Thus, the truncated CI wave functions possess incorrect electronic character, and as shall be seen later, also a contaminated spatial symmetry, hence, the wrong SOC behavior.

Table 8 shows the same type of SOC calculations, based on a single reference CI wave function, for the pyramidalization mode. Here the situation is less severe than in the case of the twist mode. Nevertheless, some overestimation in comparison with the MCSCF results is apparent in the CISD wave function, but CISDT is already reasonable. Apparently, the diradical character of the singlet wave function at the pyramidalized geometry is less pronounced than in the 90°-twisted geometry where the pure diradical character is required by symmetry.

D. A Practical Minimal Model for SOC Calculations. Since a straightforward truncated CISD, etc., fails to produce reasonable SOC trends, we turned to the original valence bond (VB) model of Salem and Rowland.[2] Following Cundari and Gordon,[33] who used Boys localization technique as an entry to VB, we have started with a triplet ROHF calculations of the ethylene molecule and followed with Boys' localization. The localization procedure leads to four σ_{CH} bond orbitals, one σ_{CC} bond orbital, and two hybrids, h_1 and h_2, each concentrated on one of the carbon atoms. The hybrids and σ_{CC} are shown in Figure 1 for the twist mode and in Figure 2 for the syn-pyramidalization mode. It is apparent that the hybrids are AOs on one carbon with a small delocalization tail on the other carbon atom, and as such are in the same spirit as the natural hybrid orbitals used by Michl[4] in his treatment of SOC in diradicals. The σ_{CC} orbital is seen to be unperturbed in the twisted ethylene, and to possess a "banana" shape in the pyramidalization mode.

These localized orbitals form a basis for a subsequent SO-CI. The simplest level uses only the AO hybrids, h_1 and h_2, and leads to a three-configuration singlet state, eq 4, and a single configuration triplet state, eq 5 (phase factor is dropped).
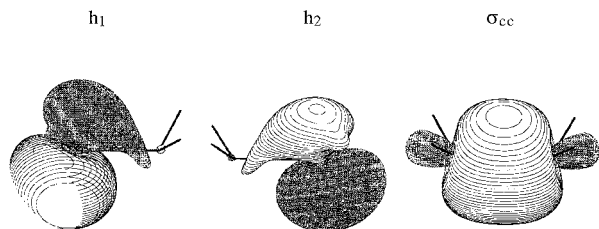
Spin−Orbit Coupling Patterns

J. Phys. Chem. A, Vol. 102, No. 29, 1998 **5929**

h₁   h₂   σ_CC

Figure 2. The h_1, h_2 hibrids and σ_{CC} orbital of C_2H_4 during the syn-pyramidalization distortion.

$$S_0 = \lambda_{cov}\{2^{-1/2}[|h_1\bar{h}_2| - |\bar{h}_1 h_2|]\} + \lambda_{ion}[|\bar{h}_1 h_1| + |h_2\bar{h}_2|] \quad (4)$$

$$T_1^{\,z} = 2^{-1/2}[|h_1\bar{h}_2| + |\bar{h}_1 h_2|] \quad (5a)$$

$$T_1^{\,x} = 2^{-1/2[|h_1 h_2| - |\bar{h}_1\bar{h}_2|]} \quad (5b)$$

$$T_1^{\,y} = 2^{-1/2[|h_1 h_2| + |\bar{h}_1\bar{h}_2|]} \quad (5c)$$

In eq 4, λ is the mixing coefficient where the subscript "cov" refers to the covalent wave function and "ion" to the ionic configurations where the two electrons occupy the same AO hybrid.

The above representation corresponds precisely to a two-configuration singlet state, described by the ϕ^2 and ϕ^{*2} MO configurations, and to a single configuration triplet state of the $\phi\phi^*$ type, where ϕ and ϕ^* correspond to the ROHF π and π^* orbitals during the twist or pyramidalization distortion. The corresponding wave functions are given in eqs 6 and 7 (phase factor is dropped).

$$S_0 = \lambda_0|\phi\bar{\phi}| - \lambda_D|\phi^*\bar{\phi}^*| \quad (6)$$

$$T_1^{\,z} = 2^{-1/2}[|\phi\bar{\phi}^*| + |\bar{\phi}\phi^*|] \quad (7a)$$

$$T_1^{\,x} = 2^{-1/2}[|\phi\phi^*| - |\bar{\phi}\bar{\phi}^*|] \quad (7b)$$

$$T_1^{\,y} = 2^{-1/2}[|\phi\phi^*| + |\bar{\phi}\bar{\phi}^*|] \quad (7c)$$

This identity has been checked and verified by running SOC calculations using the $\{h_1,h_2\}$ and $\{\phi,\phi^*\}$ orbital sets. These states are similar to the those obtained from an MCSCF(ϕ/ϕ^*) wavefunction, as the one used by Caldwell et al.,[7c] with the exception that the MCSCF orbitals are optimized for the singlet state. Indeed, the $\langle SOC\rangle$ obtained with the ROHF orbital set is larger than the SOC obtained by the MCSCF set (especially with the larger basis set, cc-pVDZ).

An advantage of the minimal models is their correct qualitative behavior upon twisting, where at 90° the singlet wave function becomes purely diradicaloid, and the reproduction of all other trends; namely, that the $\langle SOC\rangle_{sp}$ is larger than the $\langle SOC\rangle_t$ and that the anti-pyramidalization mode leads to zero $\langle SOC\rangle$. Thus, the simplest model is very useful for understanding qualitative trends. In the case of the twist mode, the simplest model is also quantitatively reasonable producing, for example, ~88% of the total SOC with the STO-3G basis set and 65% with the split basis sets (see also footnote c in Table 9). However, for the pyramidalization mode, the minimal model is quantitatively less satisfactory, producing, for example, only ~50% of the total SOC in STO-3G. Adding the σ_{CC} orbital to the $\{h_1,h_2\}$ set hardly changes the $\langle SOC\rangle_t$ values for the twist distortion, but improves markedly those for the pyramidalization

TABLE 9: Comparison $\langle SOC(Z^*)\rangle$ Values Calculated using the Minimal Model,[a] with $\langle SOC(BP)\rangle$ Results

	$\langle SOC\rangle$/cc-pVDZ	
geometry, Θ	$\langle SOC(Z^*)\rangle^{b,c}$	$\langle SOC(BP)\rangle$
(I) Twist Mode		
T_1, 0	0.0	0.0
T_1, 10	0.30	
T_1, 30	0.82	
T_1, 40	1.00 (1.40)	1.43
T_1, 50	1.07 (1.43)	1.57
T_1, 60	1.03 (1.37)	1.58
T_1, 70		
T_1, 90	0.0	0.0
(II) Syn-Pyramidalization Mode^{b,c}		
T_1, 0	0.0	0.0
T_1, 50	3.90 (5.20)	4.50
T_1, 70	4.26 (5.68)	5.30
T_1, 90	4.25 (5.67)	5.77

[a] The orbital set used in these calculations is $\{h_1, h_2, \sigma\}$. [b] In parentheses are results multiplied by $^4/_3$. [c] Similar trends are obtained with other basis sets. For example, with STO-3G, at 50° twist $\langle SOC\rangle_t = 0.52$ cm^{-1}, while at 70° pyramidalization $\langle SOC\rangle_{sp} = 3.37$ cm^{-1}. With STO-6G, the corresponding value are 0.56 and 3.56 cm^{-1}, while with 6-31G these are 1.12 and 4.04 cm^{-1}.
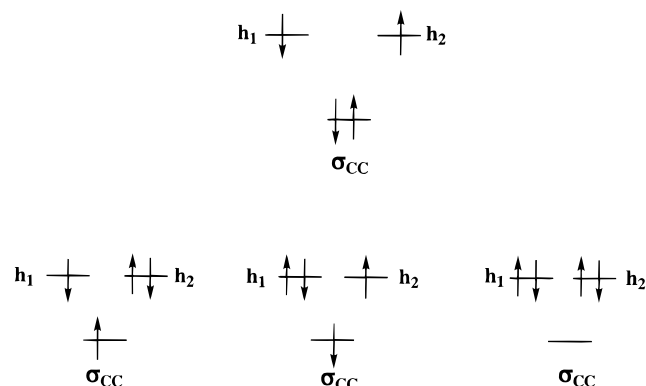

Figure 3. Electronic configurations based on the $\{h_1, h_2, \sigma_{CC}\}$ orbital set of C_2H_4 (see Figures 1 and 2). Strong configuration mixing is expected in the pyramidalization distortion.

distortion. This effect highlights the importance of the $\pi-\sigma$ mixing during the pyramidalization distortion. Indeed, the wave function shows significant mixing of configurations which involve electron shift from the σ_{CC} orbital to the hybrids as depicted in Figure 3. In contrast, these configurations have a negligible weight (<0.001) during the twist distortion. Inclusion of σ_{CC} in the orbital basis set is equivalent to adding more one-center SOC interactions. The importance of these configurations in the syn-pyramidalization mode, as opposed to the twist mode further highlights that the SOC of the latter mode involves significant interference of one-center and two-center interactions while the pyramidalization mode is one-center dominated.

Table 9 collects the $\langle SOC(Z^*)\rangle$ values calculated at the common minimal model, based on the $\{\sigma_{CC},h_1,h_2\}$ orbitals set, alongside the $\langle SOC(BP)\rangle$ results. The results of the $\{\sigma_{CC},h_1,h_2\}$ model are 65−74% of the benchmark values for the twist mode and 74−87% for the syn-pyramidalization mode. Applying a single average factor ($^4/_3$) produces results (in parentheses) which deviate moderately from the $\langle SOC(BP)\rangle$ results. Thus, while the minimal effective model is not spectacular, it is nevertheless reasonable and attractive in view of the marginal CPU cost of these calculations, in comparison with all others.

E. One- and Two-Center SOC Interaction in the Twist and Pyramidalization Distortions. In order to assess the

TABLE 10: One-Center and Full $\langle$SOC$\rangle$ Values. Dependence on the Basis Sets and the Type of Calculations for the Twist Distortion

	spin−orbit coupling, $|\langle S_0|H_{SO}|T_1\rangle|$, cm^{-1}								
	$\langle$SOC(Z^*)$\rangle_t$, MCSCF(12/12)^a						$\langle$SOC(BP)$\rangle_t$, MRD-CI^b		
	STO-3G			cc-pVDZ			TZP		
geometry, Θ	full	one-center	ratio^c	full	one-center	ratio^c	full	one-center	ratio^c
T$_1$, 0	0.0	0.0		0.0	0.0				
T$_1$, 10	0.16	0.05	0.309	0.48	0.45	0.924			
T$_1$, 30	0.44	0.13	0.299	1.33	1.23	0.923			
T$_1$, 40	0.54	0.16	0.290	1.64	1.51	0.923	1.71	1.73	1.015
T$_1$, 50	0.59	0.17	0.279	1.81	1.67	0.923	1.88	1.92	1.019
T$_1$, 60	0.58	0.16	0.267	1.83	1.69	0.923	1.89	1.94	1.023
T$_1$, 70	0.49	0.13	0.256	1.60	1.47	0.920			
T$_1$, 90	0.0	0.0		0.0	0.0				

^{a} H$_{SO}$ is effective 1e operator with $Z^* = 3.6$. ^{b} H$_{SO}$ is Breit−Pauli 1e+2e operator. ^{c} One-center/full.

TABLE 11: One-Center and Full $\langle$SOC$\rangle$ Values. Dependence on the Basis Sets and the Type of Calculations for the Syn-Pyramidalization Distortion

	spin−orbit coupling, $|\langle S_0|H_{SO}|T_1\rangle|$, cm^{-1}								
	$\langle$SOC(Z^*)$\rangle_{sp}$, MCSCF(12/12)^a						$\langle$SOC(BP)$\rangle_{sp}$, MRD-CI^b		
	STO-3G			cc-pVDZ			TZP		
geometry, Θ	full	one-center	ratio^c	full	one-center	ratio^c	full	one-center	ratio^c
T$_1$, 0	0.0	0.0		0.0	0.0				
T$_1$, 10	1.09	1.02	0.935	1.43	1.38	0.965			
T$_1$, 30	3.02	2.81	0.931	4.02	3.84	0.956			
T$_1$, 40							4.08	4.04	0.990
T$_1$, 50	4.36	4.05	0.928	5.99	5.64	0.942	4.83	4.76	0.985
T$_1$, 60							5.39	5.31	0.986
T$_1$, 70	5.23	4.88	0.933	7.47	6.98	0.933	5.82	5.78	0.993
T$_1$, 90	5.87	5.55	0.946	8.60	8.06	0.937	6.29	6.33	1.006

^{a} H$_{SO}$ is effective 1e operator with $Z^* = 3.6$. ^{b} H$_{SO}$ is Breit−Pauli 1e+2e operator. ^{c} One-center/full.

relative importance of the one- and two-center SOC interactions, we have calculated them separately using both the approximate one-electron method, as well as the full Breit−Pauli method. Table 10 shows the results for the twist distortion at the geometry of the triplet state: $\langle$SOC(Z^*)$\rangle_t$ values for STO-3G and cc-pVDZ basis set at the full valence MCSCF level, alongside the $\langle$SOC(BP)$\rangle_t$ values at the MRCI/cc-pVDZ level. The $\langle$SOC(Z^*)$\rangle_t$ results show that the two-center terms are dominant with the STO-3G basis set, but the trend is reversed with the larger basis set where the 1-center terms constitute 92% of the total $\langle$SOC(Z^*)$\rangle_t$. Practically similar results are obtained when $\langle$SOC(Z^*)$\rangle_t$ is calculated with the singlet geometry. Moreover, there is a strong dependence of the one-center/two-center ratio on the level of computation with any basis set. Thus, with a minimal MCSCF(2/2), the one-center interaction dominates the $\langle$SOC(Z^*)$\rangle_t$ with both basis sets, while with full valence MCSCF, the two-center dominates when the basis set is STO-3G, and with the cc-pVDZ the contribution of the two-center increases by 0.41 cm^{-1} at the singlet geometry.

The $\langle$SOC(BP)$\rangle_t$ values in Table 10 show dominance of the one-center terms. However, for *the singlet geometry the two-center terms can reach as much as 20% of the total $\langle$SOC-(BP)$\rangle_t$*. Clearly, the twist distortion exhibits a significant interference of one- and two-center terms, and this interplay is particularly acute for the small basis set, and not at all negligible for the larger basis set. This interplay is likely to be the origin of the success of the STO-3G basis set to reproduce $\langle$SOC(Z^*)$\rangle$ values for mono-carbon species and failure to do so for the ethylene.

Table 11 displays the results for the syn-pyramidalization mode. In this case, it is apparent that the one-center interaction dominates the $\langle$SOC(Z^*)$\rangle_{sp}$ and $\langle$SOC(BP)$\rangle_{sp}$ values even with the small basis set. Furthermore, the $\langle$SOC$\rangle_{sp}$ value does not

TABLE 12: Partition of the One- and Two-Electron Parts of $\langle$SOC$\rangle$ into One-Center and Two-Center Contributions

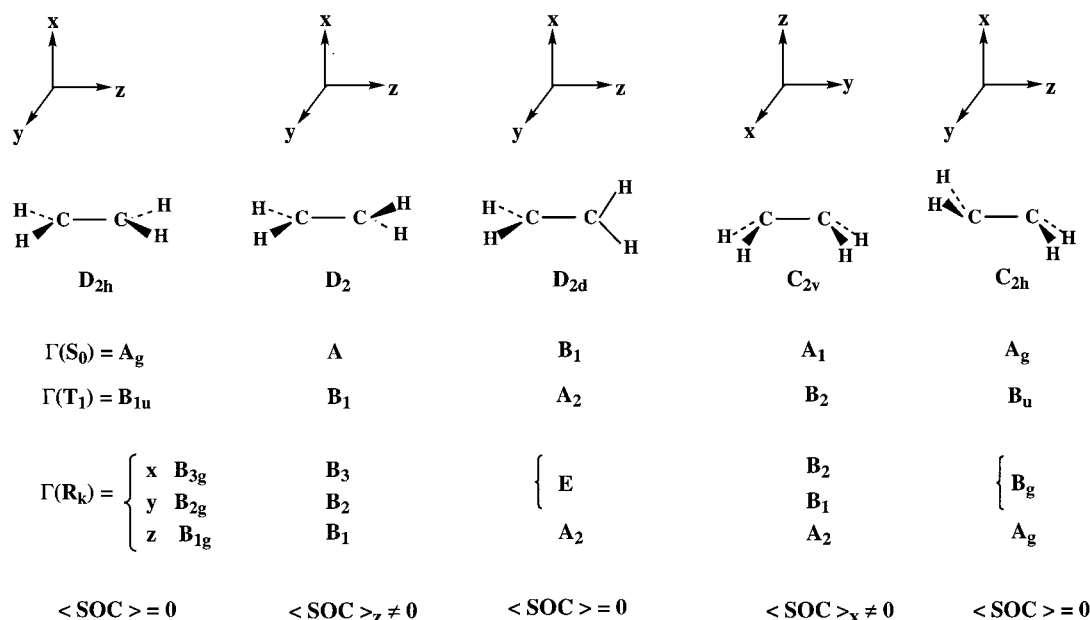|					
	$\langle$SOC(BP)$\rangle^{a,b}$, cm^{-1}				
		1e		2e	
geometry, Θ	full	one-center	two-center	one-center	two-center
	Twist Mode				
T$_1$, 40	1.707	3.342	−0.085	−1.610	0.061
T$_1$, 50	1.884	3.699	−0.089	−1.780	0.054
T$_1$, 60	1.893	3.713	−0.080	−1.777	0.037
S$_0$, 40	2.055	4.806	−0.672	−2.356	0.276
S$_0$, 50	2.181	5.026	−0.643	−2.453	0.252
S$_0$, 60	2.183	4.913	−0.535	−2.383	0.188
	Pyramidalization Mode				
T$_1$, 20	2.194	4.202	−0.010	−2.023	0.024
T$_1$, 40	4.078	7.688	0.151	−3.647	−0.115
T$_1$, 50	4.833	9.014	0.298	−4.253	−0.226
T$_1$, 60	5.389	9.995	0.434	−4.683	−0.358
T$_1$, 70	5.823	10.820	0.504	−5.040	−0.461
T$_1$, 80	6.154	11.470	0.571	−5.331	−0.555
T$_1$, 90	6.294	11.797	0.597	−5.463	−0.638

^{a} TZP basis set. ^{b} See Table 1 for geometries.

exhibit any strong dependence of the one-center/two-center ratio on the level of calculations (e.g., in minimal vs full valence MCSCF). Evidently, unlike the twist distortion, the pyramidalization mode is dominated by strong one-center terms. As such, the STO-3G basis set can produce reasonable $\langle$SOC(Z^*)$\rangle_{sp}$ values and there is less dependence on the computational level.

Table 12 shows the relative contributions of the one- and two-electron $\langle$SOC(BP)$\rangle$ parts to the one-center and two-center interactions. As observed before,[1d,g,4] the one- and two-electron contributions are differently signed; the latter being ca. 50% of the former. This recurring result supports the general view that

Spin−Orbit Coupling Patterns

J. Phys. Chem. A, Vol. 102, No. 29, 1998 **5931**

SCHEME 2

$\Gamma(S_0) = A_g$	A	B_1	A_1	A_g
$\Gamma(T_1) = B_{1u}$	B_1	A_2	B_2	B_u

$$\Gamma(R_k) = \begin{cases} x & B_{3g} \\ y & B_{2g} \\ z & B_{1g} \end{cases} \qquad \begin{matrix} B_3 \\ B_2 \\ B_1 \end{matrix} \qquad \begin{cases} \quad E \\ A_2 \end{cases} \qquad \begin{matrix} B_2 \\ B_1 \\ A_2 \end{matrix} \qquad \begin{cases} B_g \\ A_g \end{cases}$$

$$\langle SOC \rangle = 0 \qquad \langle SOC \rangle_z \neq 0 \qquad \langle SOC \rangle = 0 \qquad \langle SOC \rangle_x \neq 0 \qquad \langle SOC \rangle = 0$$

the two-electron part acts as a screening factor on the one-electron SOC interaction.

Further inspection of Table 12 reveals again that the SOC generated by the syn-pyramidalization mode is dominated one-center interaction, while the two-center interactions nearly cancel out. In contrast, the SOC generated by the twist distortion exhibits a small one-center interaction and a two-center interaction which is sensitive to the C−C distance. As the distance decreases from 1.50 to 1.33 Å (T_1 to S_0 geometry), the two-center SOC becomes significant and does not cancel out.

In summation: the SOC(BP) associated with the twist distortion exhibits interference of one- and two-center SOC interactions, while that of the syn-pyramidalization is virtually dominated by the one-center interaction. This conclusion is in line with the SOC(Z^*) results in Tables 10 and 11.

IV. Discussion

The foregoing results project a few main trends which require explanation: (a) The specific dependence of $\langle SOC \rangle$ on the symmetry of the distortion mode; namely, the origins of the zero $\langle SOC \rangle$ for the twist mode at 90° and for the anti-pyramidalization mode. A related trend is the apparent vector additivity of $\langle SOC \rangle$ due to mono-pyramidalization distortions: (b) The root cause of the significant $\langle SOC \rangle_{sp}$ for the syn-pyramidalization mode in contrast with the weak $\langle SOC \rangle_t$ promoted by the twist mode, at any computational level. (c) The capricious behavior of $\langle SOC \rangle_t$ with basis set and wave-function level, in contrast with the more consistent behavior of the $\langle SOC \rangle_{sp}$ values, as far as one-center vs two-center terms are concerned.

In what follows we shall present a simple qualitative model, which accounts for these trends and suggest a mnemonic which allows to visualize the SOC interactions. Our qualitative model will rely on the minimal orbitals set, used above in eqs 4−7.

A. Symmetry Analysis. We begin with a well-known,[1] but nonetheless essential symmetry analysis of the SOC matrix element, $\langle T_1|\mathbf{H}_{SO}|S_0\rangle$, because this analysis provides information which is independent of the level of calculation. Being part of the total Hamiltonian, the spin−orbit Hamiltonian behaves as the totally symmetric representation, Γ_1, of the molecular point group. Therefore a nonzero SOC matrix element requires that

the direct product of the state symmetries will contain the totally symmetric representation, eq 8.[1b]

$$\Gamma(S_0) \otimes \Gamma(T_1^V) \otimes \Gamma(R_k) = \Gamma_1 + ... \rightarrow \langle SOC \rangle_k \neq 0; \quad k = x, y, z \tag{8}$$

Here, $\Gamma(T_1^V)$ is the representation of the spatial wavefunction of the triplet state, while $\Gamma(R_k)$ is the representation of the triplet spin wave functions, which behave like the real rotations R_k of the point group. Thus, a k-component of SOC will be generated when the condition in eq 8 can be fulfilled.

Scheme 2 summarizes the symmetry properties for the various distorted geometries of ethylene following eq 8. It is seen that, in D_{2h}, D_{2d}, and C_{2h} point groups, none of the direct products meets the condition in eq 8. In contrast, in D_2, which corresponds to a twist of less than 90°, and in C_{2v}, which corresponds to a syn-pyramidalization, one of the $\langle SOC \rangle$ components meets the condition in eq 8 and, hence, is nonzero. Furthermore, it is possible to show that, in D_{2d}, the only singlet state which possesses the B_1 symmetry assigned to S_0 is the purely diradical state, whereas the higher lying purely ionic singlet has A_1 symmetry. A singlet state which contains ionicity in D_{2d} must therefore be symmetry contaminated of mixed $B_1 + A_1$ character. This is precisely the situation with CISD wave function of a 90° twisted ethylene which contains a large amount of the ionic character, leading thereby to the erroneous result that there is a nonzero $\langle SOC \rangle_t$ (Table 6), which would have vanished had the CISD wave function had the correct symmetry. Only the MRCI and MCSCF wave functions possess the correct symmetry properties.

It is apparent that the symmetry analysis provides a straightforward binary type classification (yes−no) of the $\langle SOC \rangle$ patterns in perfect accord with the computational finding. However, this information alone is insufficient to answer the quantitative questions. This insight is provided by electronic structure consideration of the $\langle SOC \rangle$ as done in the following section.

B. Electronic Structure Analysis of $\langle SOC \rangle$. To model the SOC matrix element, we restrict ourselves to the wave functions based on the minimal orbital set, as defined above by eqs 4−7, and use the one-electron SO operator with an effective nuclear

SCHEME 3
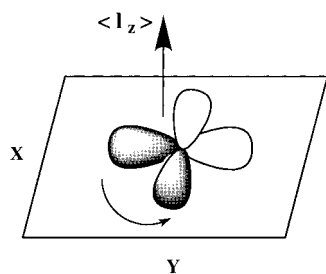
$$\langle p_x|l_z|p_y\rangle = i\,\hbar < p_x \mid p_x >$$

charge (which for our qualitative purposes is a constant). The k-component ($k = x, y, z$) of SOC is given by eq 9.

$$\langle T_{1k}|H_{SO}(Z^*)|S_0\rangle = \langle SOC_k\rangle = Af(\lambda)\langle a|l_k/r^3|b\rangle \quad (9)$$

$$f(\lambda) = \lambda_{ion}: \quad a, b = h_1, h_2 \quad (10a)$$

$$f(\lambda) = \lambda_0 - \lambda_D: \quad a, b = \phi, \phi^* \quad (10b)$$

Here, A is a term which contains all the constants, while $f(\lambda)$ is a function of the CI coefficients and is specified in eqs 10a and 10b. Thus, in eq 10a this function is equal to the ionic coefficient in the singlet wave function in the VB type representation, eqs 4 and 5, and the orbitals $\langle a|$ and $|b\rangle$ are in turn the hybrids h_1 and h_2. In eq 10b, $f(\lambda)$ corresponds to the difference between the coefficients of the fundamental and doubly excited MO configurations (eq 6), and the orbitals are in turn the ϕ and ϕ^* MOs, which in the planar ethylene are simply π and π^*, and otherwise modified by the specific distortion.

The insight gained by use of the two orbital sets is complementary, and the choice of the orbital set depends ultimately on the type of insight one requires. Thus, for example, using the VB model with the two hybrids $\{h_1,h_2\}$ one can immediately see that for the twist distortion at 90°, the ground singlet state becomes purely diradical with $\lambda_{ion} = 0$ so that the $\langle SOC\rangle_t$ vanishes, as argued before by Salem and Roland[2] and by Michl.[4] The same conclusion is reached by using the two-configuration MO model. Thus, at a 90° twist the coefficient of the fundamental and doubly excited configurations are equal[19] and since $\lambda_0 - \lambda_D = 0$ in eq 10b, then the $\langle SOC\rangle_t$ vanishes. In the following discussion we shall make use of both models, but rely initially on the two-configuration MO model.

A maximum expectation value for $\langle I_k\rangle$ is obtained when the orbitals are mutually perpendicular, while the k-axis is the normal to their plane (see Scheme 3). For example, an x, y orbital relationship will generate a nonzero $\langle l_z\rangle$ and hence a z-component of SOC, etc. Both the twist and pyramidalization distortions create perpendicular orbital relationships and can therefore promote SOC. Let us then analyze the two modes in detail.

$\langle SOC\rangle_t$ *Patterns for Twist and Syn-Pyramidalization Modes. Twist Distortion.* The orbital rehybridization induced by twisting is depicted schematically in Figure 4, where it is seen that the ϕ and ϕ^* MOs arise from admixture of the original $\pi(x)$ and $\pi(x)^*$ orbitals with the symmetry-matched in-plane $\sigma(y)$ and $\sigma(y)^*$ orbitals of the CH_2 moieties. The resulting expression for the ϕ and ϕ^* orbitals are eqs 11a and 11b, where the 1s orbitals on the H atoms have been deleted since they do not contribute to SOC, and where the asterisked
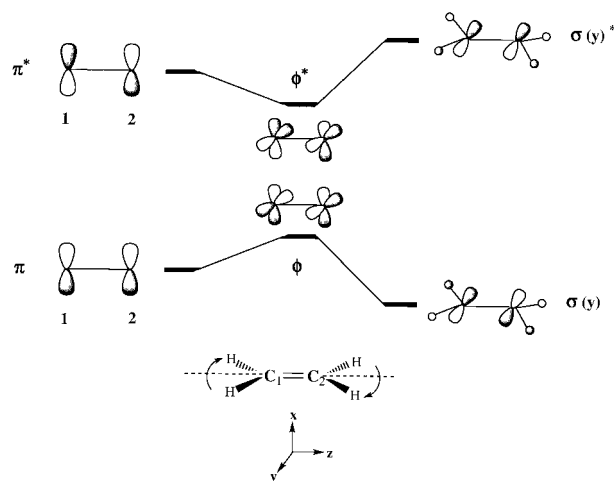

Figure 4. The ϕ and ϕ^* orbitals which are nascent from the π and π^* orbitals upon twist distortion of C_2H_4. The shapes of ϕ and ϕ^* are determined by mixing of π and π^* with the symmetry matched in-plane orbitals $\sigma(y)$ and $\sigma(y)^*$. Only significant orbital mixing is shown.

coefficients signify their association with the out-of-phase MO ϕ^*.

$$\phi = c_x(x_1 + x_2) - c_y(y_1 - y_2) \quad (11a)$$

$$\phi^* = c_x^*(-x_1 + x_2) + c_y^*(y_1 + y_2) \quad (11b)$$

The x, y AO relationship in the two MOs will generate in turn a z-component of SOC, which from eq 9 leads to the following SOC expression:

$$\langle SOC_z\rangle_t = A(\lambda_0 - \lambda_D)\{2(c_yc_x^* - c_xc_y^*)\zeta_C - 2(c_yc_x^* + c_xc_y^*)(\zeta_{12}^\pi + \zeta_{21}^\pi)\} \quad (12)$$

Here the ζ terms are the SOC integrals defined over AOs, where ζ_C is the one-center integral (i.e., the atomic constant[1] and ζ_{12}^π is the two-center SOC interaction which couples orbitals in a π-type overlapping situation).[2,3] Thus, the SOC in the twist mode is given by an interplay of one- and two-center interactions, weighted by the difference and sum of products of the AO coefficients in the MOs, ϕ and ϕ^*, as well as by the configuration mixing coefficients term.

The dependence of $\langle SOC_z\rangle_t$ upon the twist angle is determined by the interplay of the configuration mixing term $(\lambda_0 - \lambda_D)$, which vanishes at 90°, and the orbital mixing coefficients, (e.g., c_y), which peak at 90°. The balance between the effects results in a maximum $\langle SOC_z\rangle_t$ around 50–60°. A simple modeling of the angular dependence of the various terms shows that both the one- and two-centers peak at the same angle, no doubt because they are weighted by the same angular terms.

The intrinsic efficacy of SOC depends on the interplay of the one- and two-center terms in eq 12. It is seen that the one-center term is weighted by a difference of coefficient products. The calculations reveal that the orbital hybridization occurs to the same extent for the π and π^* MOs, such that the mixing coefficients c_y and c_y^* in eq 12 are virtually equal. As such, the one-center term will be given by eq 13 and will depend on the difference between the AO coefficients in the π and π^* MOs.

$$\langle SOC_z\rangle_{t,1-center} = 2c_yA(\lambda_0 - \lambda_D)(c_x^* - c_x)\zeta_C \quad (13)$$

$$\langle SOC_z\rangle_{t,2-center} = -4c_yA(\lambda_0 - \lambda_D)(c_x^* + c_x)\zeta_{12}^\pi \quad (14)$$

Since this difference is small, and since the mixing coefficient

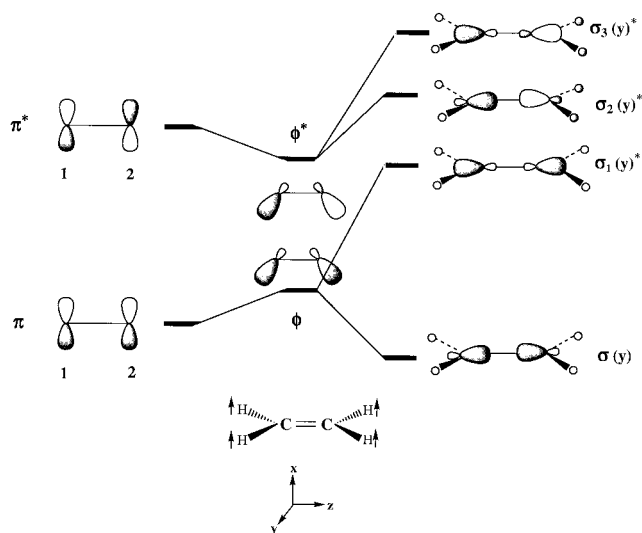Spin−Orbit Coupling Patterns

J. Phys. Chem. A, Vol. 102, No. 29, 1998 **5933**

Figure 5. The ϕ and ϕ^* orbitals which are nascent from the π and π^* orbitals upon syn-pyramidalization of C_2H_4. The shapes of ϕ and ϕ^* are determined by mixing of π and π^* with the symmetry matched σ and σ^* orbitals of the C−C and C−H bonds, designated as $\sigma(y)$ and $\sigma(y)^*$. Only significant orbital mixing is shown.

c_y which weighs the entire term is itself small (0.2−0.3 at 50° twist), the one-center contribution in the twist distortion will be residually small. In contrast, the two-center term in eq 14 is weighted by a sum of coefficient products, which is a significant factor. Thus, even though the two-center integrals themselves, ζ_{12}, are much smaller than the one-center integral ζ_C, the ratio of the weighing coefficients is large enough to make the two-center terms significant. It is evident from Tables 10 and 11 that, for small basis sets (e.g., STO-3G), the ζ_{12} contribution is sizeable, but decreases in importance for extended basis sets.

As a digression, it is instructive to inspect eq 13 and to consider the one-center term in an orbital approximation where overlap is neglected in the normalization constant. In this case, $c_x^* = c_x$, the one-center SOC contribution completely vanishes, and the entire $\langle SOC_z \rangle_t$ would have been made from the two-center contribution in eq 14. This is the approximation which guided the initial model of Salem and Rowland[2] and later of Shaik and Epiotis,[3] as well as more recently of Su.[5] It is remarkable that both the one-center and two-center terms peak at about the same twist angle and their symmetry and distance behavior is identical. Consequently, the result derived in the Salem−Rowland model for ethylene, by consideration of the two-center terms, was found by Michl[4] and by Carlacci et al.[7a] to match well the behavior deduced from detailed SOC calculation.

Syn-Pyramidalization Distortion. The orbital rehybridization in Figure 5 shows that, upon pyramidalization (note the change in the coordinate system), the original $\pi(z)$ and $\pi(z)^*$ MOs mix in $\sigma(y)$ and $\sigma(y)^*$ MOs of the C−C and C−H varieties. The resulting expression for the ϕ and ϕ^* orbitals are eqs 15a and 15b. The coefficients of the 1s orbitals on the H atoms do not contribute to SOC, but their size affects eventually the magnitude of the coefficients c_y and c_y^*.

$$\phi = c_z(z_1 + z_2) - c_y(y_1 - y_2) \qquad (15a)$$

$$\phi^* = c_z^*(z_1 - z_2) - c_y^*(y_1 + y_2) \qquad (15b)$$

The y, z AO relationship in the two MOs will generate in turn an x-component of SOC, which by applying eq 9 becomes

$$\langle SOC_x \rangle_{sp} = A(\lambda_0 - \lambda_D)\{2(c_yc_z^* - c_zc_y^*)\zeta_C -$$
$$2(c_yc_z^* + c_zc_y^*)(\zeta_{12}^\sigma + \zeta_{21}^\pi)\} \qquad (16)$$

The various terms in eq 16 are analogous to those derived for the twist mode above. Here too the $\langle SOC_x \rangle_{sp}$ is determined by 1- and 2-center terms weighted by products of coefficients and by the configuration mixing coefficients, $(\lambda_0 - \lambda_D)$.

The behavior of $\langle SOC_x \rangle_{sp}$ along the pyramidalization distortion is determined by the balance of the configuration mixing term $(\lambda_0 - \lambda_D)$ and the orbital mixing coefficient c_y. In contrast to the twist mode, the $(\lambda_0 - \lambda_D)$ term does not vanish even at the maximum of the distortion at 90°. In addition, the orbital mixing increases as the pyramidalization angle increases. Consequently, $\langle SOC_x \rangle_{sp}$ increases gradually and peaks at 90°.

Unlike the case of the twist mode, here the calculations show that c_y is much larger than c_y^*. This relationship originates in the different mechanisms of orbital mixing in Figure 5. Thus, here ϕ is generated by a sandwich orbital interaction where π mixes in antibonding and bonding fashions, respectively, with the $\sigma(y)$ and $\sigma_1(y)^*$ type orbitals. Bonding and antibonding is defined with respect to the overlap of the p_z AOs with the hydrogen 1s AOs. Consequently, the sandwich orbital interaction results in a nonbonding situation where the 1s coefficients almost cancel out, while the p_y contributions to the orbital add up. In contrast, the ϕ^* orbital arises by mixing of two $\sigma(y)^*$ orbitals into $\pi(z)^*$ in a bonding fashion, and the result is an increased contribution of the 1s AOs on H at the expense of the p_y AOs, which now tend to cancel out due to opposing contributions from the two $\sigma(y)^*$ orbitals.

This orbital mixing pattern is the root cause why c_y is much larger than c_y^*. Since the coefficients of the $\pi(z)$ and $\pi^*(z)$ obey the relation $c_z^* > c_z$, the ratio of $c_yc_z^*/c_zc_y^*$ in eq 16 is large (e.g., 2.4 at 50°). For the sake of simplicity, we neglect the $c_zc_y^*$ term in eq 16 and obtain the one-center contribution as follows in eq 17, while the corresponding two-center term is given by eq 18.

$$\langle SOC_x \rangle_{sp,1-center} = 2Ac_yc_z^*(\lambda_0 - \lambda_D)\zeta_C \qquad (17)$$

$$\langle SOC_x \rangle_{sp,2-center} = -2Ac_yc_z^*(\lambda_0 - \lambda_D)(\zeta_{12}^\pi + \zeta_{12}^\sigma) \qquad (18)$$

Clearly, the one-center $\langle SOC_x \rangle_{sp}$ is determined now by a single dominant term, and since the one-center integral ζ_C is large, the syn-pyramidalization distortion will be dominated by the one-center SOC interaction. Furthermore, CI, which includes excitation from and to the $\sigma(y)$ type MOs (see, e.g., Figure 3), will add additional one-center terms and increase the $\langle SOC_x \rangle_{sp}$ interaction. This is the reason why the minimal practical model for the pyramidalization mode has to include the σ_{CC} orbital in the evaluation of SOC by CI (Table 9).

At this point, the main SOC patterns which have been obtained computationally are lucid. What remains to formulate is *a simple pictorial model* for adding the SOC contributions and to rationalize the trends without resort to equations. This is done in next section.

C. A Pictorial Model for Molecular SOC Interactions in Organic Species. A nonzero SOC requires a nonzero orbital angular momentum which can couple with the spin angular momentum. A nonzero angular momentum requires, in turn, an electron to shift between two perpendicular p-AOs.[2−4] This shift creates a unit of angular momentum along an axis which is perpendicular to the plane spanned by the AOs. An illustration is given in Scheme 3, where the two AOs are p_x and p_y, and the electron shift from x to y creates a unit of angular

SCHEME 4
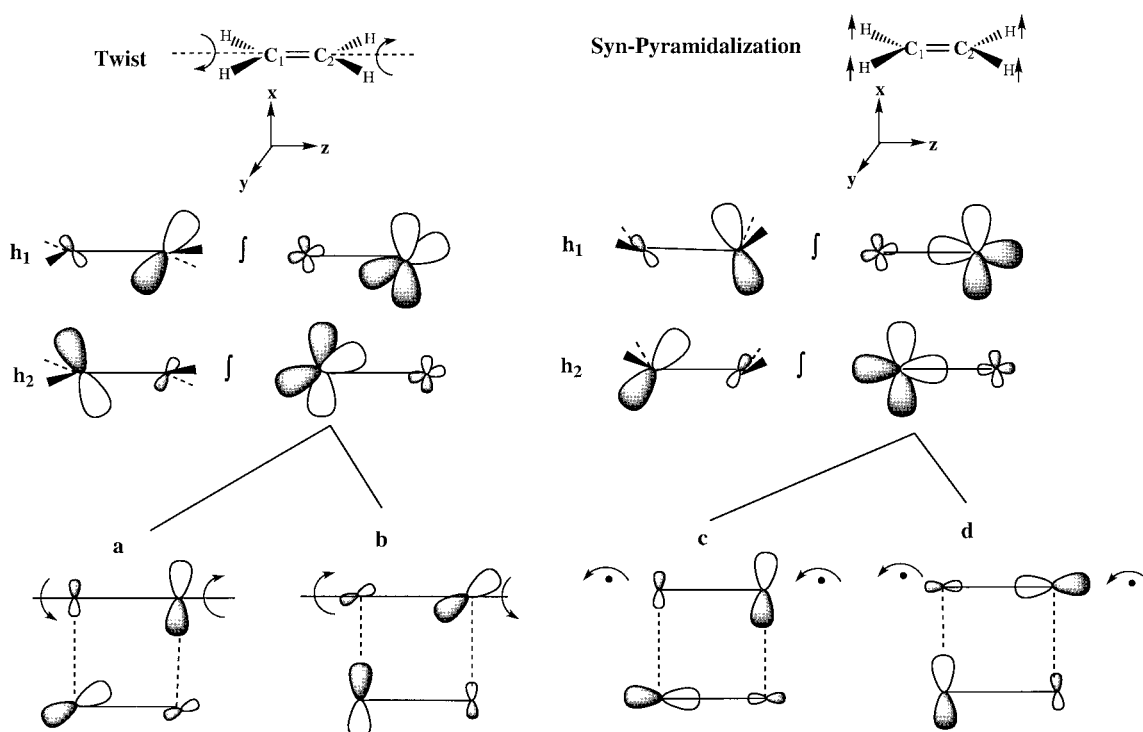
momentum in the *z*-direction. For the sake of convention, the direction of the rotation is decided by matching the shaded lobes of the orbitals, and the resulting angular momentum points in the positive direction (like the direction of a right-handed screw axis). This unit of angular momentum, which is centered on the nucleus (or nuclei in a two-center case) can now couple with a codirectional spin vector (whose origin is on the electron), and thereby create a nonzero *z*-component of SOC.

This well-known description[1-5] can be generalized for any pair of perpendicular p-AOs. Thus, all we need to do in molecular systems is to draw the orbitals which participate in the SOC and to determine the directions of the angular momentum vectors produced by *the orbital rotations needed to match the shaded lobes*. When these vectors add up, there will result a large SOC and vice versa when they are produced in opposite directions. To illustrate the applicability of this simple picture, we use the model with the hybrid orbital set $\{h_1, h_2\}$. Before doing so, however, it is important to qualify that having an electron shift SOC matrix element, between triplet and singlet states, requires that the wave functions will differ by the occupancy of a single spin orbital. This will occur only when the singlet state has an ionic contribution (i.e., $\lambda_{ion} \neq 0$ in eq 10a). Since the λ_{ion} changes with the distortion (e.g., $\lambda_{ion} = 0$ at a 90° twist), the result is that the molecular SOC will not generally peak at 90° AO relationship, but at a compromise angle. This however, does not affect the intrinsic requirement, for perpendicular AO relation, of the angular momentum expectation value.

With these qualifications in mind, let us proceed to analyze the SOC promoted by the twist and syn-pyramidalization modes, using the pictorial representation of the angular momentum matrix element, $\langle h_1|l_k|h_2 \rangle$. Scheme 4 shows the hybrid orbitals h_1 and h_2 which are obtained from the calculations. Each hybrid includes a small delocalization tail, in an antibonding relation to the main lobe on the other carbon. To visualize lucidly, we decompose these hybrids to their AO components as shown to the right of the hybrids. Now it is apparent that each AO

component set in one hybrid has a perpendicular component set in the other hybrid.

To obtain the angular momenta, we have now to draw the AO component sets in the two hybrids, and to trace the rotations that match the AOs of the two sets, henceforth *an orbital rotation diagram*. By the choice of the centers to be matched by the orbital rotation, the diagram mnemonic deduce vectors corresponding to one-center or two-center. The orbital rotation diagrams **a**−**d** show the directions of orbital rotations which are required to match the shaded lobes of the perpendicular components on the same carbon site. As such, **a**−**d** exemplify the use of the diagram for one-center terms. Matching the lobes on opposite sites will provide the two-center terms.

Diagrams **a** and **b** show the orbital rotations required in the twist distortion. It is seen that the rotations come in opposite directions for the two sites, and hence, the one-center angular momentum vectors for the twist mode will have opposite directions and will contribute small net SOC interaction. In **c** and **d**, we show the orbital rotation diagrams for the syn-pyramidalization distortion. Here it is seen that the rotations are both in the same direction, and as such the syn-pyramidalization distortion will produce a significant one-center SOC interaction. Thus, orbital rotation diagrams project lucidly the difference between the distortions. It is easy to construct the orbital rotation diagrams for the two-center interactions and to verify that the corresponding SOC terms add up, and as such interfere with the residual one-center interaction in the twist mode. It is also easy to verify that the anti-pyramidalizaion leads to zero SOC.

Conclusions

A detailed study of the SOC mechanisms which couple the triplet $\pi\pi^*$ state (T_1) to the singlet ground state (S_0) in ethylene enables to gain considerable insight into the qualitative and quantitative trends of the SOC matrix elements. Three computational methods were used: the full Breit−Pauli (BP) SOC

Spin−Orbit Coupling Patterns

J. Phys. Chem. A, Vol. 102, No. 29, 1998 **5935**

Hamiltonian[1g] the one-electron mean-field (MF) operator,[22] and the approximate one-electron operator[21] that uses an effective nuclear charge Z^*. The MF treatment was found to work as well as the full BP treatment. The approximate one-electron method provides good qualitative trends, but the constancy of Z^* is questionable whenever two-center terms become significant. Indeed, the MF operator may be interpreted as having a variable Z^* parameter which responds to the molecular environment and geometry. This may well be the root cause of the good performance of the MF one-electron operator in the present case. Should this performance prove routine, it will then provide solid grounds for computing and conceptualizing SOC with a one-electron philosophy.

Two archetype distortion modes of ethylene were considered: the twist mode which changes the symmetry from D_{2h} to D_2 and then to D_{2d}, and pyramidalization modes which change the ethylene symmetry to C_{2v} (syn-pyramidalization) or C_{2h} (anti-pyramidalization). A mono-pyramidalization distortion was also tested.

It is shown that, unlike mono-carbon species where even an STO-3G basis set is sufficient to obtain good SOC values using $Z^* =3.6$ in the approximate one electron operator, in ethylene one must use a large basis set, at least of the double-ζ quality. Furthermore, the poor performance of the STO-3G basis set is more accentuated in the twist mode, while the SOC promoted by the syn-pyramidalization mode is reasonably well reproduced. The quality of the wave function used for S_0 and T_1 is also crucial, but again more so for the twist mode where single reference CI wave functions lead to faulty results, even if one uses as much as CISDTQ expansion of the CI. In contrast, MCSCF (even minimal) and MRCI wave function perform correctly. A practical minimal model, which involves three active orbitals in the CI, the σ_{CC}, orbital and the two localized hybrids on the carbon atoms, was tested with the approximate one-electron method and was proved to reproduce the qualitative trends and make fair quantitative estimates of SOC.

It is found that both the twist and syn-pyramidalization distortions of ethylene promote a nonzero SOC interaction, which involves an interplay between one-center and two-center SOC terms. In the twist distortion, the interplay is strong because the one-center terms arise from a residual incomplete cancellation of the two on-site interactions. In contrast, in the syn-pyramidalization distortion the interplay is weak, because the one-center terms add up. Consequently the syn-pyramidalization promotes SOC matrix elements which exceed 6 cm^{-1}, while the twist mode has a weaker SOC of the order of 2 cm^{-1}. Zero SOC is obtained for distortion which involve either a 90° twist or an anti-pyramidalization.

A qualitative analysis based on symmetry and electronic structure enables to understand these trends, as detailed in the discussion section. A simple physical model which enables to carry out the vectorial summation of SOC in a pictorial manner is constructed and is used to explain the trends in the twist and syn-pyramidalization modes.

Interestingly, the one- and two-center terms exhibit the same qualitative behavior and hence making predictions using two-center terms alone (e.g., as done in studies of Salem and Roland,[2] Shaik and Epiotis,[3a] and Su[5]) lead to the similar conclusions, even if the one-center terms are dominant.

Finally, due to the dominant one-center term associated with the pyramidalization distortion, this mode can promote a significant SOC interaction. Thus, in accord with conclusions by Caldwell et al.,[7c] the pyramidalization distortion may assist in the $T_1 \rightarrow S_0$ decay mechanisms of locked olefins (e.g., **1** and

2). Furthermore, the stereoselective behavior of the pyramidalization distortion (syn vs anti) makes the syn-pyramidalization a good candidate for producing stereoselective cyclobutanes in 2+2 cycloaddition, as predicted by Shaik and Epiotis.[3a] It remains to ascertain that pyramidalization modes can also lead to T_1-S_0 surface crossing where the decay is most efficient and where the stereochemical requirements associated with SOC may be expressed.

References and Notes

(1) General sources for discussions of SOC are (a) Lefebvre-Brion, H.; Field, R. W. *Perturbations in the Spectra of Diatomic Molecules*; Academic Press: New York, 1986. (b) McGlynn, S. P.; Azumi, T.; Kinoshita, M. *Molecular Spectroscopy of the Triplet State*; Prentice-Hall: Englewood-Cliffs, NJ, 1969. (c) Matsen, F. A.; Klein, D. J. *Adv. Photochem.* **1969**, *7*, 1. (d) Richards, W. G.; Trivedi, H. P.; Cooper, D. L. *Spin-Orbit Coupling in Molecules*; Clarendon Press: Oxford, 1981. (e) Ross, R. B.; Christiansen, R. A. *Adv. Quantum Chem.* **1988**, *19*, 139. (f) Lower, K. S.; El-Sayed, M. A. *Chem. Rev.* **1966**, *66*, 199. (g) Hess, B. A.; Marian, C. M.; Peyerimhoff, S. D. In *Molecular Electronic Structure*; Yarkony, D. R., Ed.; World Scientific: Singapore, 1995; part I, p 152−278. (h) Langhoff, S. R.; Kern, C. W. In *Modern Theoretical Chemistry*; Schaeffer, H. F., III, Ed.; Plenum Press: New York, 1977; Vol 4. (i) Marian, C. M. In *Problem Solving in Computational Molecular Science: Molecules in Different Environments*; Wilson, S., Dieckersen, G. H. F., Eds.; Kluwer: Dordrecht, 1997.

(2) Salem, L.; Rowland, *Angew. Chem.*, *Int. Ed. Engl.* **1972**, *11*, 92.

(3) (a) Shaik, S. S.; Epiotis, N. D. *J. Am. Chem. Soc.* **1978**, *100*, 18. (b) Shaik, S. S. *J. Am. Chem. Soc.* **1979**, *101*, 2736. (c) Shaik, S. S. *J. Am. Chem. Soc.* **1979**, *101*, 3184. (d) Shaik, S. S.; Epiotis, N. D. *J. Am. Chem. Soc.* **1980**, *102*, 122. (e) Larson, J. R.; Epiotis, N. D.; McMurchie, L. E.; Shaik, S. S. *J. Org. Chem.* **1980**, *45*, 1388.

(4) Michl, J. *J. Am. Chem. Soc.* **1996**, *118*, 3568.

(5) Su, M.-D. *J. Phys. Chem.* **1996**, *100*, 4339.

(6) Zimmerman, H. E.; Kutateladze, A. G.; Maekawa, Y.; Mangette, J. E. *J. Am. Chem. Soc.* **1994**, *116*, 9795. Zimmerman, H. E.; Kutateladze, A. G. *J. Org. Chem.* **1995**, *60*, 6008. Zimmerman, H. E.; Kutateladze, A. G. *J. Am. Chem. Soc.* **1996**, *118*, 249.

(7) (a) Carlacci, L.; Doubleday, C.; Fourlani, T. R.; King, H. F.; McIver, J. W., Jr. *J. Am. Chem. Soc.* **1987**, *109*, 5323. (b) King, H. F.; Furlani, T. R. *J. Comput. Chem.* **1988**, *9*, 771. (c) Caldwell, R. A.; Carlacci, L.; Doubleday, C.; Furlani, T. R.; King, H. F.; McIver, J. W., Jr. *J. Am. Chem. Soc.* **1988**, *110*, 6901.

(8) (a) Morita, A.; Kato, S. *J. Phys. Chem.* **1992**, *96*, 1067. (b) Morita, A.; Kato, S. *J. Phys. Chem.* **1993**, *97*, 3298.

(9) Amatatsu, Y.; Morokuma, M.; Yabushita, S. *J. Chem. Phys.* **1991**, *94*, 4858.

(10) (a) Amatatsu, Y.; Yabushita, S.; Morokuma, M. *J. Chem. Phys.* **1994**, *100*, 4894. (b) Yabushita, S.; Morokuma, M. *Chem. Phys. Lett.* **1990**, *175*, 518.

(11) (a) Manna, M. R.; Yarkony, D. R. *J. Chem. Phys.* **1991**, *95*, 1808. (b) Manna, M. R.; Yarkony, D. R. *Chem. Phys. Lett.* **1992**, *188*, 352.

(12) (a) Armentrout, P. B. *Science* **1991**, *251*, 175. (b) Armentrout, P. B. *Annu. Rev. Phys. Chem.* **1990**, *41*, 313.

(13) Weisshaar, J. C. *Acc. Chem. Res.* **1993**, *26*, 213.

(14) Schröder, D.; Schwarz, H. *Angew. Chem.*, *Int. Ed. Engl.* **1995**, *34*, 1973.

(15) (a) Danovich, D.; Shaik, S. *J. Am. Chem. Soc.* **1997**, *119*, 1770. (b) Fiedler, A.; Schröder, D.; Shaik, S.; Schwarz, H. *J. Am. Chem. Soc.* **1994**, *116*, 10734. (c) Shaik, S.; Danovich, D.; Fiedler, A.; Schröder, D.; Schwarz, H. *Helv. Chim. Acta* **1995**, *78*, 1393.

(16) (a) Clemmer, D. E.; Chen, Y.-M.; Khan, F. A.; Armentrout, P. B. *J. Phys. Chem.* **1994**, *98*, 6522. (b) Chen, Y.-M.; Clemmer, D. E.; Armentrout, P. B. *J. Am. Chem. Soc.* **1994**, *116*, 7815.

(17) Schröder, D.; Schwarz, H.; Clemmer, D. E.; Chen, Y.; Armentrout, P. B.; Baranov, V. I.; Bohme, D. K. *Int. J. Mass Spectrom. Ion Processes* **1997**, *161*, 175.

(18) Goodman, J. L.; Peters, K. S.; Misawa, H.; Caldwell, R. A. *J. Am. Chem. Soc.* **1986**, *108*, 6803.

(19) Gemein, B.; Peyerimhoff, S. D. *J. Phys. Chem.* **1996**, *100*, 19257.

(20) For applications of the Breit-Pauli Hamiltonian, see: (a) Hippe, D.; Peyerimhoff, S. D. *J. Chem. Phys.* **1992**, *96*, 3503. (b) de Vivie, R.;

Peyerimhoff, S. D. *J. Chem. Phys.* **1989**, *90*, 3660. (c) de Vivie, R.; Peyerimhoff, S. D. *J. Chem. Phys.* **1988**, *89*, 3028. (d) Klotz, R.; Peyerimhoff, S. D. *Mol. Phys.* **1986**, *57*, 573. (e) Matsushita, T.; Klotz, R.; Marian, C. M.; Peyerimhoff, S. D. *Mol. Phys.* **1987**, *62*, 1385. (f) Thümmel, H.; Klotz, R.; Peyerimhoff, S. D. *Chem. Phys.* **1989**, *135*, 229. (g) Hess, B. A.; Buenker, R. J.; Marian, C. M.; Peyerimhoff, S. D. *Chem. Phys. Lett.* **1982**, *89*, 459. (h) de Vivie, R.; Marian, C. M.; Peyerimhoff, S. D. *Chem. Phys.* **1987**, *112*, 349.

(21) For example, see: (a) Koseki, S.; Schmidt, M. W.; Gordon, M. S. *J. Phys. Chem.* **1992**, *96*, 10768. (b) Koseki, S.; Gordon, M. S.; Schmidt, M. W.; Matsunaga, N. *J. Phys. Chem.* **1995**, *99*, 12764.

(22) (a) Hess, B. A.; Marian, C. M.; Wahlgren, U.; Gropen, O. *Chem. Phys. Lett.* **1996**, *251*, 365. (b) Marian, C. M.; Wahlgren, U. *Chem. Phys. Lett.* **1996**, *251*, 357.

(23) Frisch, M. J.; Trucks, G. W.; Schlegel, H. B.; Gill, P. M. W.; Johnson, B. G.; Robb, M. A.; Cheeseman, J. R.; Keith, T. A.; Peterson, J. A.; Montgomery, J. A.; Raghavachari, K.; Al-Laham, M. A.; Zakrzewski, V. G.; Ortiz, J. V.; Foresman, J. B.; Cioslowski, J.; Stefanov, B.; Nanayakhara, A.; Challacombe, M.; Peng, C. Y.; Ayala, P. Y.; Chen, W.; Wong, M. W.; Andres, J. L.; Replogle, E. S.; Gomperts, R.; Martin, R. L.; Fox, D. J.; Binkley, J. S.; Defrees, D. J.; Baker, J.; Stewart, J. J. P.; Head-Gordon, M.; Gonzalez, C.; Pople, J. A. Gaussian, Inc.: Pittsburgh, PA, 1995.

(24) (a) Buenker, R. J.; Peyerimhoff, S. D. *Theor. Chim. Acta* **1974**, *35*, 33. (b) *Theor. Chim. Acta* **1975**, *39*, 217. (c) Buenker, R. J.; Peyerimhoff, S. D.; Butscher, W. *Mol. Phys.* **1978**, *35*, 771.

(25) Dunning, T. H. *J. Chem. Phys.* **1989**, *90*, 1007.

(26) Dunning, T. H. *J. Chem. Phys.* **1971**, *55*, 716. Huzinaga, S. *J. Chem. Phys.* **1965**, *42*, 1293.

(27) Widmark, P.-O.; Malmqvist, P.-Å.; Roos, B. O. *Theor. Chim. Acta* **1990**, *77*, 291.

(28) (a) Marian, C. M. Ph.D. Dissertation, University of Bonn, 1980. (b) Hess, B. A. *Ph*.D. Dissertation, University of Bonn, 1980. Both are available from the library of The University of Bonn.

(29) For example of GAMESS-USA, revision Feb 1995, see: Schmidt, M. W.; Baldridge, K. K.; Boatz, J. A.; Elbert, S. T.; Gordon, M. S.; Jensen, J. H.; Koseki, S; Matsunaga, N.; Nguyen, K. A.; Su, S. J.; Windus, T. L.; Dupuis, M.; Montgomery, J. A. *J. Comput. Chem.* **1993**, *14*, 1347.

(30) Huber, K. P.; Herzberg, G. *Molecular Spectra and Molecular Structure*; Van Nostrand Reinhold, Co.: New York, 1979; Vol. IV, p 144.

(31) Moore, C. E. *Atomic Energy levels*; NSRDS-NBS35; U.S. Government Printing Office: Washington, DC, 1971.

(32) Klotz, R.; Marian, C. M.; Peyerimhoff, S. D.; Hess, B. A.; Buenker, R. J. *Chem. Phys.* **1983**, *76*, 367.

(33) Cundari, T. R.; Gordon, M. S. *J. Am. Chem. Soc.* **1991**, *113*, 5231.